Dalton Transactions

Insight into selectivity: Uptake studies of radionuclides $^{90}Sr^{2+}$, $^{137}Cs^{+}$, and $^{233}UO_2^{2+}$ with bis-amidoxime polymers

Journal:	*Dalton Transactions*
Manuscript ID	DT-ART-12-2017-004935.R1
Article Type:	Paper
Date Submitted by the Author:	11-Mar-2018
Complete List of Authors:	Piechowicz, Marek; The University of Chicago, Department of Chemistry Chiarizia, Renato; Argonne National Laboratory , Chemical Sciences and Engineering Soderholm, L.; Argonne National Laboratory, Chemical Sciences and Engineering Division

Journal Name

ARTICLE

Insight into selectivity: Uptake studies of radionuclides $^{90}Sr^{2+}$, $^{137}Cs^{+}$, and $^{233}UO_2^{2+}$ with bis-amidoxime polymers

Received 00th January 20xx,
Accepted 00th January 20xx

DOI: 10.1039/x0xx00000x

Marek Piechowicz[a,b], R. Chiarizia[a], and L. Soderholm[a,*]

Uptake characteristics by a bis-amidoximated polymer are presented for $^{90}Sr^{2+}$, $^{137}Cs^{+}$, and $^{233}UO_2^{2+}$ to assess rational ligand design and polymer engineering efforts applied to selective uranium extraction. Functionalized with the bis-amidoxime diaryl ether ligand at a loading of 1.98 mmol per gram polymer, the polymer was found to sorb uranium from a pH 6 solution with a separation factor (α) over cesium of $1.2 \cdot 10^3$. Strontium uptake was negligible throughout the pH range studied whereas cesium uptake averaged <30%. Moreover, at near neutral pH, the sorbent was able to purify water to below the the United States' set maximum contaminant level for uranium, decreasing the U concentration from 330 ppb to below 3 ppb in 30 minutes. Density functional theory (DFT) calculations, used to probe the nature of the metal-bis-amidoxime interaction, help inform the empirically realized uptake selectivity.

Introduction

Functionalized solid-phase sorbent materials play an important role in chemical separations, particularly when more classic methods such as solvent extraction are impractical or ineffective.[1–6] Potential sorbent applications include environmental sequestration for the purpose of either pollutant remediation or trace-constituent isolation, where functionalized solid-phase sorbents have the advantages of high analyte selectivity and ease of handling. An example of trace-constituent isolation is the longstanding interest in the use of solid-phase sorbents for the extraction of uranium from seawater, driven by the need to secure adequate nuclear-fuel resources to meet future energy requirements.[7–9]

Solid-phase sorbents including metal-organic frameworks (MOFs),[10–13] inorganic hybrids such as layered metal sulfides,[14] and functionalized polymers[15] all constitute materials of interest as agents to effect chemical separations. Functionalized polymers, in the form of amidoxime-functionalized (-R=NNH$_2$OH) braided fibers[16] and diphosphonate-functionalized resins[17] in particular, have garnered recent interest for use in the extraction of uranium from seawater and actinide separation from mixed waste.[18] Preliminary investigations of amidoxime-metal binding in aqueous solutions[19] yielded high stability constants for uranyl-acetamidoxime complexes, on the order of $\boldsymbol{\beta_{11} \sim 10^{10}}$, corroborating earlier studies[20] which suggested that amidoxime based polymers are among the only materials suited for uranium uptake from aqueous solutions. Moreover, follow-up work[19] demonstrated that uranium uptake by amidoxime functionalized polymers was selective over Co^{2+}, Ni^{2+}, and Zn^{2+} with empirical selectivity factors (α) on the order of ~10^3 for Co^{2+}, Ni^{2+} and ~10^4 for Zn^{+2}. Recently published studies investigating the tridentate analogue of diamidoxime—glutarimidedioxime—confirm this trend in selectivity of UO_2^{2+} over Ni^{2+}.[21] For uranium from seawater applications, where VO_2^{+} is the main competitor for U binding sites,[22] bis-amidoxime functionalized polymers enjoy an advantage, with selectivity factors of U over V of approaximately 3 (corresponding to a 5:1 w/w U to V uptake ratio).[9]

Extending the investigation of selective uranium binding, we describe herein the uranium uptake characteristics of a bis-amidoxime functionalized polymer, comparing its performance with uptake results of selected alkali and alkaline earth metal cations. Whereas many studies have hitherto focused on the design and synthesis of amidoxime based materials for uranium sequestration from seawater under seawater-specific conditions, the purpose of this work is to more fully investigate the selectivity of amidoxime for uranium with particular emphasis placed on pH, buffer effects, and competing ions. Results show that >99% uranium was sorbed from an acetate buffered solution with a maximum distribution ratio of $\boldsymbol{1.4 \cdot 10^5}$ mL g^{-1}. Studies with ^{90}Sr and ^{137}Cs were conducted to investigate the uptake behavior of larger mono- and divalent cations which have typically caused problems in solid-phase sorbent materials by competing for available binding sites.[23] Strontium uptake is negligible throughout the pH range studied whereas cesium uptake averages less than 30% from solution under acidic or basic conditions and effectively zero under the near neutral conditions of interest. The uptake studies are in good agreement with computational work used to predict the order of selectivity.

[a] Chemical Sciences and Engineering Division, Argonne National Laboratory, Argonne, IL 60439, United States. Email: LS@anl.gov
[b] Department of Chemistry, University of Chicago, 5640 S Ellis Ave., Chicago, Illinois 60637, United States.

† Electronic Supplementary Information (ESI) available: Detailed Counting Methods, Cartesian Coordinates of optimized coordination complexes, Buffer Calculations, Comparison of Amidoximated Sorbent Performance. See DOI: 10.1039/x0xx00000x

Scheme 1: Synthesis of bis-amidoxime functionalized polymer

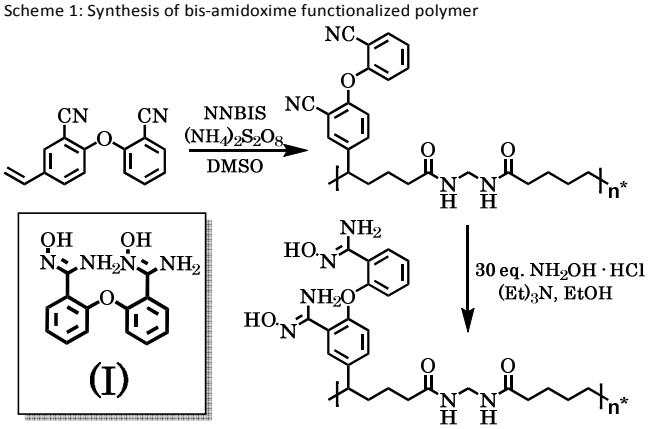

Experimental Details

Caution! Materials used herein are radioactive and as such are considered health risks. Their use requires proper facilities, correct PPE, and appropriate training.

Materials

Nitric acid was ACS reagent grade and used as received. All water used for uptake experiments was obtained from a Milli-Q2 system with a measured resistivity of at least 18 MΩ. Radiochemical experiments were performed using solutions of ^{90}Sr, ^{137}Cs, and ^{233}U obtained from ANL stock. The ^{233}U stock was 30.6 mM in 1M HNO_3. The ^{90}Sr stock was in aqueous solution. The ^{137}Cs stock was 87 µM in 0.01 M HNO_3. All other reagents including liquid scintillation counting cocktail, sodium acetate, and ammonium hydroxide were used as received.

The chemical structure and synthesis of the bis-amidoximated polymer used for uptake studies is shown in Scheme 1. Full synthetic details and characterization of the polymer material can be found in previous work.[9] In brief, vinylated dicyano diaryl ether was copolymerized with *N,N'*-methylenebis(acrylamide) (NNBIS) to afford a hydrophilic crosslinked polymer with dicyano loading of 1.98 mmol per gram polymer. Treatment with hydroxylamine hydrochloride in ethanol afforded the bis-amidoxime species (Scheme 1).

Density Functional Theory (DFT) Methods

All calculations utilized the Gaussian 16RevA.03 quantum chemistry program[24] with DFT at the B3LYP[25,26] level of theory. All light atoms were modeled by the 6-311+G* basis set. Cs and Sr were modeled using the LANL2DZ effective core potential while U was modeled with the Stuttgart RSC 1997 relativistic effective core potential, known in the literature to yield reasonable geometries and thermodynamics of metal-ligand species.[27–29] The protocols used in this work are appropriate for all atoms studied including uranium and represent standard methods used by the community to investigate such coordination complexes.[30–32] Solvation with water was modeled using the conductor-like polarizable calculation model (CPCM) unless gas phase explicitly stated.[33] Generally, complexes were geometrically optimized first and then subjected to frequency calculations and natural bond orbital (NBO) analysis using the same basis set and level of theory. For thermodynamic calculations, the following equations were used:

$$M^n + L^a \longrightarrow ML^{n+a} \quad (1)$$

$$\Delta G_{reaction} = \Sigma\,(\Delta G_{products}) - \Sigma\,(\Delta G_{reactants}) \quad (2)$$

The quantum theory of atoms in molecules (QTAIM) approach was explored using the Multiwfn program version 3.3.9.[34,35] Electron density, the Laplacian of electron density, the energy density at bond critical points, Wiberg, and Laplacian Bond Indices were calculated with Multiwfn 3.3.9.

Uptake Studies

Uptake studies were conducted in 10 mL glass vials with ~1 mg polymer at a phase ratio of 1 mg polymer per 1 mL spiked solution. Radionuclides were spiked in such a way to yield A_0 <10 000 cpm 100 µL^{-1}. Samples were shaken for 30 minutes on a plate shaker at 500 rpm prior to centrifugation and syringe filtration (Whatman, PVDF, 0.2 µm pore size). Empirically, distribution ratios were calculated according to the following equation:

$$\mathbf{D_{W,exp}} = \frac{\mathbf{A_{0,corr}} - \mathbf{A_{F,corr}}}{\mathbf{A_{F,corr}}} * \frac{\mathbf{V}}{\mathbf{m}} \quad (3)$$

Where $\mathbf{A_{0,corr}}$ is the background corrected initial counts as determined by alpha/beta or gamma counting, $\mathbf{A_{F,corr}}$ is the background corrected final counts post-uptake, V is the volume of the solution in µL, and m is the mass of the polymer in mg. In all cases, approximately 1 mg of polymer was used with a phase ratio of 1 mg mL^{-1}.

Buffers were prepared according to standard procedures found in the literature. The alkaline pH region (pH 8-10) was attained with an ammonium buffer ($[NH_3]$ + $[NH_4^+]$ = 0.01 M). The near neutral pH region (pH 4-7) was attained with a sodium acetate buffer ($[CH_3COO^-]$ + $[CH_3COOH]$ = 0.01 M). Acidic conditions (pH = 2, 3) were attained with HNO_3 at the proper concentration. Conditions below pH = 2 were not investigated due to filtration difficulties encountered at higher acidities.

Complexing ion concentration was calculated for the acetate ligand used as part of the buffer media. Significant deviations in D_w values obtained with (3) have been corrected using the procedure outlined in the Supporting Information. Corrected and uncorrected values are included in Figure 4 below.

Owing to the challenge of accurately determining pK_a values of amidoxime groups on polymers,[36] we chose a broad pH range to study metal ion uptake. Best estimates suggest the protonated-neutral proton transfer occurs around pH ~5.5 and the neutral-anionic transition occurs around pH ~10.[37] Exploring uptake over a wide pH range allows us to investigate the performance of the amidoximated polymer over a range of potential protonation states and to make accurate comparisons with state-of-the-art materials for U uptake from water, which are typically studied at near neutral conditions.

Radiometric Measurements

Alpha and beta counting were performed via liquid scintillation on a Packard Model 2000 CA counter using an LSC cocktail volume of 5 mL. Gamma counting was performed using a Packard Cobra Autogamma counter. Counting methods used for each isotope can be found in the Supporting Information (Table S1). Regions of interest (ROIs) were individually selected for each isotope to include highest intensity emissions.

Results and Discussion

In Silico Studies of bis-amidoxime coordination complexes

DFT calculations were performed on Sr, Cs, and U complexed bis-amidoxime species. Various starting geometries were investigated to assess optimized structures and provide a reasonable representation of the metal coordination environment on the polymer. Optimized structures obtained for Sr, Cs, and U complexes with the bis-AO ligand (**I**) in different protonation states are shown in Figures 1, 2, and 3. Corresponding Cartesian coordinates are provided in the Supporting Information. In most cases, starting geometries consist of (A) one metal ion near one amidoxime, (B) one metal ion in a binding pocket, (C) one metal ion near each amidoxime, and (D) one metal ion near amidoxime and one in a binding pocket. In these instances, the binding pocket is taken to be the region between the amidoximes where a metal can interact with both functional groups and the central diaryl ether oxygen. It was originally hypothesized that uranium would be strongly bound by the amidoxime ligands[38] and that both cesium and strontium would be excluded from strong binding on account of their larger ionic radii. However, since methylenebisacrylamide was used as the crosslinker in the original polymer synthesis, some Cs and Sr uptake was expected.

^{90}Sr.

Strontium is bound by the deprotonated bis-amidoxime ligand in a monodentate fashion in plane with the amidoxime oxygen at a distance of 2.51 Å (SI Table S3). Upon protonation, the metal rotates below the plane of the amidoxime and the corresponding Sr-O bond length increases to 2.79 Å, similar to Sr-O distances in Sr-NO_2 published structures.[39] Further protonation maintains the bonding geometry but lengthens the Sr-O distance by 0.2 Å to 2.98 Å as expected. The complexation reaction between the bis-amidoxime ligand and strontium according to equation 1 and equation 2 is exergonic for the deprotonated ligand and endergonic for both the neutral and positive states. The reaction between strontium and deprotonated bis-amidoxime is the only one that occurs spontaneously at room temperature (Table 1).

The QTAIM approach was used to provide more insight into the binding character of bis-amidoxime and strontium. Specifically, the electron density (ρ), the Laplacian of the electron density ($\nabla^2\rho$), and the energy density at a bond critical point ($H(r)$) were calculated using the Multiwfn program with DFT optimized structures as discussed above. These metrics have been successfully used in the literature to evaluate metal ligand binding in solid sorbent materials.[40] The electron density (ρ) at the critical point between Sr and the amidoxime oxygen decreases from 0.032 a.u. to 0.017 a.u. to 0.010 a.u. as the bis-amidoxime ligand undergoes successive protonation (SI Table S3). In general, values of ρ > 0.20 a.u. suggest a greater degree of covalency in comparison with ρ values < 0.10 a.u. which suggest a greater degree of ionic character. Using these guides, the Sr-O interaction can ostensibly be considered ionic in character although other metrics including long Sr-O distances suggest a non-bonding interaction. The Laplacian of electron density ($\nabla^2\rho$), the divergence of the gradient of electron density over *xyz* space, is positive in all three cases and decreases as expected. Negative (positive) values for $\nabla^2\rho$ would suggest covalent (ionic) character. Finally, the energy density at bond critical points ($H(r)$) serves as another check of bond character. Positive values are suggestive of ionic bond character and are observed for each Sr-O interaction in these cases.

	Sr^{2+}		
ΔG (kcal mol^{-1})	bis-AO^{-1}	bis-AO	bis-AO^{+1}
(A) 1 Sr	**-6.217**	**6.079**	**9.716**
(B) 1 Sr in binding pocket	**5.425**	**8.897**	**7.039**
(C) 2 Sr	**1.881**	**13.668**	**20.175**
(D) 2 Sr, only 1 in binding pocket	**13.296**	**18.652**	

Table 1. Thermodynamics of Sr-bis-AO complexes

Natural Bond Orbital (NBO) analysis was performed in order to obtain natural population analysis on the metal centers of interest. In all three Sr complexes above, the natural charge on the Sr deviates insignificantly from the expected value of +2.0 corroborating the non-bonding interactions observed. Wiberg and Laplacian bond indices were calculated using the Multiwfn program. Wiberg bond indices (WBIs) often correlate well with formal bond order while the Laplacian bond order (LBO) correlates well with *covalent* bond order. The WBIs for the Sr-O bond steadily decrease in magnitude from 0.33 to 0.19 to 0.14 upon successive ligand protonation. Concurrently, the LBO remains a small, positive value below 0.06, further suggesting the lack of covalent character in the Sr-O interactions.

Initially placing the strontium within the binding pocket of the bis-amidoxime chelator yields optimized structures wherein the strontium lies above the plane of the diaryl ether oxygen, with the smallest (largest) angular deviation apparent in the deprotonated (protonated) complex (Figure 1). Long Sr-C**O**C bond distances, on the order of 3.3 to 4.1 Å, suggest limited influence of the diaryl ether oxygen. In both deprotonated and neutral cases, the amine nitrogen exhibits a binding interaction with the Sr metal ion with WBIs of 0.26 and 0.19 respectively. Thermodynamics of complexation do not improve with binding pocket geometry, with an average Gibbs free energy change of approximately +7 kcal mol^{-1} (Table 1). For comparison, the complexation of strontium cation with dicyclohexano-18-crown-6, a ligand with demonstrated affinity for Sr,[41,42] was also studied with DFT under identical conditions. The

optimized structure gave a ΔG of -7.01 kcal mol^{-1}, signifying that strontium complexation is favorable at room temperature.

The addition of another strontium to form complexes wherein each amidoxime binds one strontium dication yields optimized structures geometrically similar to the mono-strontium cases

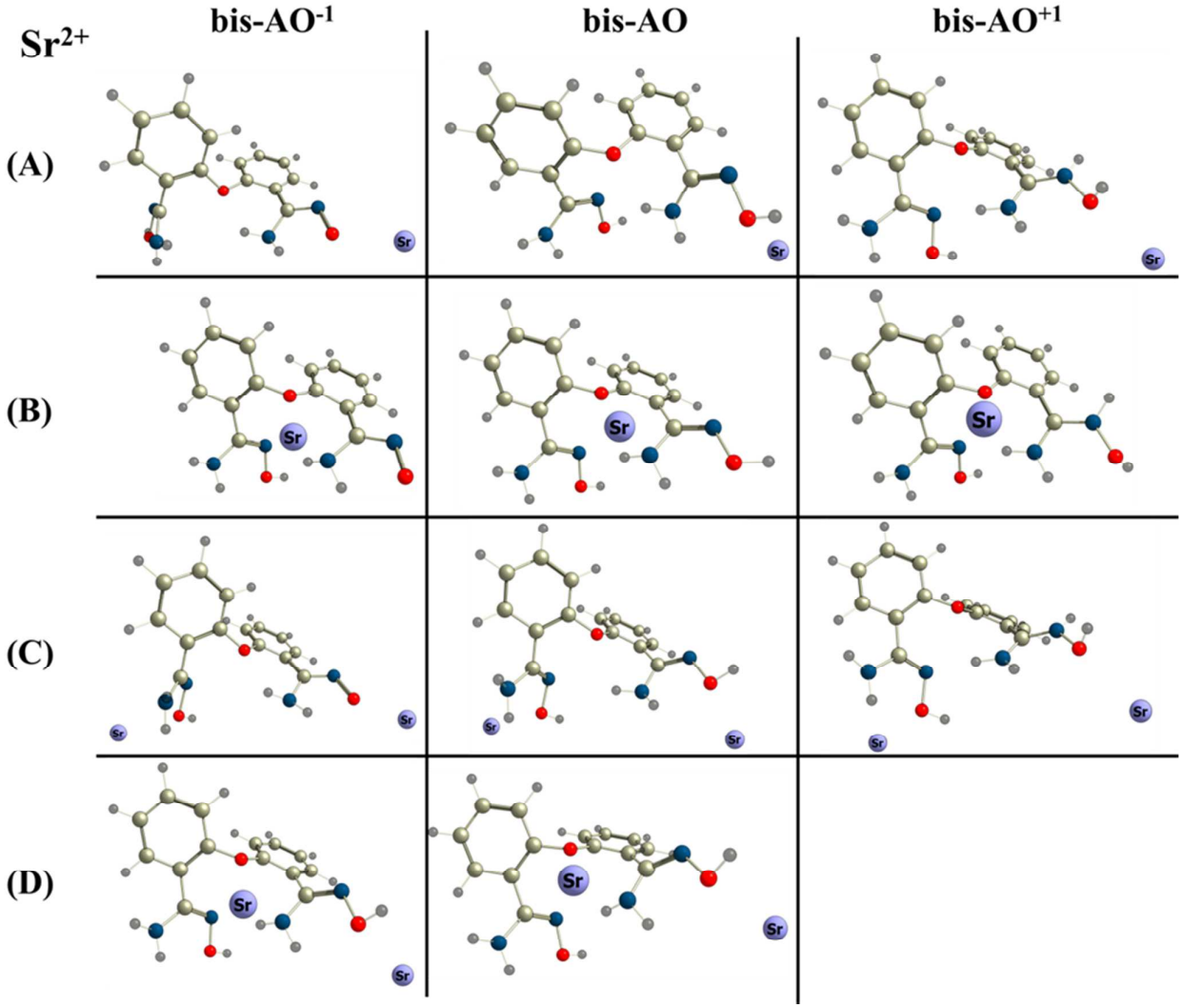

Fig. 1 Geometrically optimized perspective structures of strontium complexes. The gray, dark gray, red, dark blue, and light blue spheres represent C, H, O, N, and Sr respectively. (A) series contains one strontium near one amidoxime as the starting geometry, (B) series contains one strontium in the binding pocket, (C) series contains one strontium near each amidoxime, and (D) series contains one strontium near amidoxime and one in the binding pocket as the starting geometry. In each case, the shortest Sr-ligand interaction is outside what is considered to be a binding interaction; consequently, lines signifying Sr-ligand bonds are not shown.

discussed above. In all cases, the Sr-O bond distance increases with increasing ligand charge and Sr associates out of the amidoxime plane with charged or neutral amidoxime species. In no case is there any amine contribution to Sr binding. WBIs suggest neither N nor O donates appreciable electron density to the Sr metal center as evidenced by an NPA on Sr close to the dication ideal of +2.0 (SI Table S4).

Placement of two strontium ions (one in binding pocket geometry and one amidoxime bound) yields optimized structures with one strontium associated with an amine in the binding pocket and one bound to the amidoxime in either monodentate or η^2 fashion in geometries consistent with the structures discussed above. The deprotonated complex yields a Sr-N and Sr-O binding geometry consistent with an η^2 interaction. The thermodynamic difference between monodentate and η^2 binding geometries is not expected to be significant based on literature precedent.[43,44] In both cases, the free energy change becomes more positive. When the bis-amidoxime ligand is neutral, the Sr-O and Sr-NH_2 interactions are approximately equivalent in strength according to WBI and LBO analysis. The positively charged bis-amidoxime with strontium in the binding pocket failed to converge, yielding the ligand internally hydrogen bonded.

The DFT results for the Sr-ligand complexes support our hypothesis that Sr does not strongly interact with the bis-amidoxime ligand. The long amidoxime-Sr bond distances observed as well as metal NPA values > 1.99 in all cases suggest negligible ligand-to-metal charge transfer. Most

importantly, except for the case in which there is one Sr bound to bis-AO^{-1}, there is no indication of a free-energy stabilization of the complex. Based on these observations we conclude that the amidoxime-Sr interactions are non-bonding regardless of the ligand's protonation state. This is largely due to a mismatch in cavity size and metal ionic radius despite geometry optimization.

^{137}Cs.

The positively charged ligand with cesium in all four unique starting geometries failed to converge, despite efforts to ease convergence criteria by switching to a quadratically convergent SCF, increasing the number of cycles, or modifying the starting geometry. This lack of convergence may result from the highly unfavorable electrostatics associated with multiple charged species as well as the large size of the cesium cation. Moreover, resulting structures yielded bis-amidoxime ligands with apparent hydrogen bonding between the amine of one amidoxime and the amine of another with cesium completely excluded from bonding. Rapid convergence was obtained for neutral and anionic species.

Cesium is η^2 bound in the anionic bis-amidoxime case with a Cs-O and Cs-N distance of 3.141 Å and 3.241 Å respectively. In contrast, cesium is bound monodentate to the oxime nitrogen with a Cs-N distance of 3.44 Å in the neutral ligand complex. The Gibbs free energy of complexation is slightly positive in both cases around 3 kcal mol^{-1} (Table 2).

Interestingly, protonation of the amidoxime increases the free energy of complexation by only <0.1 kcal mol^{-1} suggesting that electrostatic interactions are not the dominant driving force in Cs complexation. Similar to the Sr cases, there is no appreciable difference between the Cs-N and Cs-O interactions in both deprotonated and neutral ligand cases. NPA values of 0.99 agree with the free ion ideal case of +1.0.

Optimized structures with cesium in binding-pocket geometry finds indistinguishable binding thermodynamics with energetics differing by about 1 kcal mol^{-1} (Table 2). Cesium as bound by the neutral ligand in binding pocket geometry situates itself 3.45 Å from the oxime oxygen and 3.60 Å from the oxime nitrogen, with WBIs suggesting a stronger Cs-N bond (Figure 2). Upon deprotonation, the ligand distorts by rotation about the Ar-O-Ar bond in order to accommodate cesium by increasing the Cs-OAr$_2$ distance from 3.41 to 6.33 Å. The resulting structure shows a Cs-amine N distance of 4.10 Å and Cs-O distance of 3.07 Å. In this case, the Cs-O interaction is stronger than the Cs-N interaction as evidenced by higher WBI and LBO bond indices. No improvement is observed to the Gibbs free energy of this ligand distortion for cesium accommodation. To compare, the interaction between cesium cation and the well-known BoBCalixC6 yields a Gibbs free energy of -56.9 kcal mol^{-1} using the same computational parameters.[45]

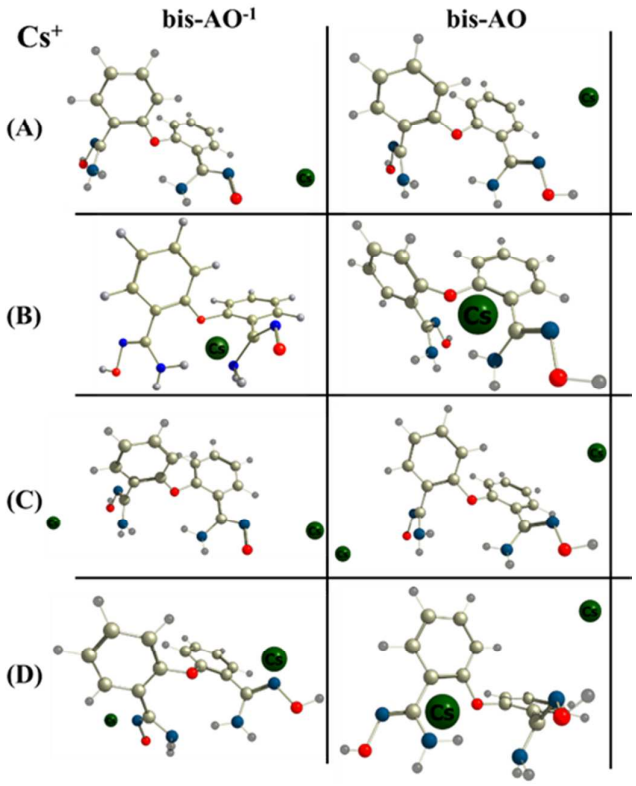

Fig. 2 Geometrically optimized perspective structures of cesium complexes. The gray, dark gray, red, dark blue, and dark green spheres represent C, H, O, N, and Cs respectively. (A) series contains one Cs near one amidoxime as the starting geometry, (B) series contains one Cs in the binding pocket, (C) series contains one Cs near each amidoxime, and (D) series contains one Cs near amidoxime and one in the binding pocket as the starting geometry

The addition of another cesium cation to the neutral complex results in monodentate coordination in plane with the oxime nitrogen or above the plane of the oxime oxygen with average bond lengths on the order of ~3.5 Å (Figure 2). Thermodynamics of complexation become less favorable by 4.3 kcal mol^{-1}. Wiberg bond indices suggest approximately equivalent Cs-O and Cs-N bonds while LBO analysis indicates that the Cs-N interaction is slightly stronger. The anionic ligand complex shows similar cesium binding with the exception that one cesium is η^2 bound. No statistically significant increase in stability is found relative to the neutral ligand complex.

Table 2. Thermodynamics of Cs-bis-AO complexes

	Cs$^+$	
ΔG (kcal mol^{-1})	bis-AO^{-1}	bis-AO
(A) 1 Cs	**2.841**	**2.918**
(B) 1 Cs in binding pocket	**3.970**	**4.126**
(C) 2 Cs	**7.290**	**8.398**
(D) 2 Cs, only 1 in binding pocket	**7.264**	**10.154**

Finally, two complexes were optimized wherein one cesium was placed in binding pocket geometry and one was placed in

close proximity to an amidoxime functional group. In the neutral ligand case, one cesium is bound in plane with an oxime nitrogen with a distance of 3.48 Å while the other is associated with the opposite face of the ligand in close proximity to the amine nitrogens of both amidoxime groups. The Gibbs free energy change of complexation becomes more positive by 1.76 kcal mol^{-1} suggesting that binding pocket geometry may be less favorable; specifically, indicating that binding two cesium cations on the same face of the ligand could be preferable. Similarly, the deprotonated ligand complex with one cesium in the binding pocket and one η^2 bound to an amidoxime yields equivalent free energies.

The positive ΔG values as well as the long Cs-amidoxime distances (~3-4 Å, SI Table S5), suggest non-bonding Cs-ligand interactions. Moreover, the small differences in the Gibbs free energy obtained upon addition of another Cs^+ demonstrate that the ligand provides no significant stabilization through geometry optimization, resulting in poor expected affinity for Cs^+ in experimental studies.

^{233}U

The uranyl dioxocation (UO_2^{2+}), by contrast, exhibits favorable thermodynamics when bound to the bis-amidoxime ligand regardless of the ligand's protonation state. Gibbs free energies decrease from -5.53 kcal mol^{-1} to -8.64 kcal mol^{-1} to -56.12 kcal mol^{-1} as the ligand undergoes successive deprotonations (Table 3). In the protonated ligand case, the uranyl cation lies parallel to the plane of the amidoxime group (Figure 3). Despite long U-O and U-N distances, NPA suggests a large degree of ligand-to-metal charge transfer with values deviating from the +6.0 ideal case by 2.8 units. This trend holds for the neutral and deprotonated ligand cases with values decreasing from 3.20 to 2.67 respectively (SI Table S6). Both neutral and anionic ligand complexes exhibit hydrogen bonding between the amine N-H and the oxime N of the adjacent amidoxime moiety despite concomitant uranyl binding.

Comparing the uranyl case with that of cesium, we find the ligand is successful in accommodating the smaller uranyl cation and unsuccessful in accommodating the much larger cesium cation. Optimized structures with uranium show intramolecular hydrogen bonding as well as strong uranium binding. The same complexes with cesium reject the metal cation *in favor of* intra-molecular hydrogen bonding.

Importantly, the addition of another uranyl increases the overall stability of the resulting complex. The free energy of complexation becomes more negative by an average of ~12 kcal mol^{-1}. In each of the three cases, there is pronounced ligand-to-metal charge transfer due to low natural charges on the metal center (< 3.24). Optimized geometries show similar U-O, U-N

bonding motifs and the persistence of intra-molecular hydrogen bonding. Uranium-amidoxime N distances average 2.42 Å, in agreement with the 2.42 Å U-N distance observed in the similar uranium-benzamidoxime crystal structure.[44] Uranium-amidoxime O distances shows greater variability with average distances of 2.56 Å compared to the 2.35 Å U-O bond distance found in the uranium-benzamidoxime complex. Laplacian Bond Indices greater than 0.67 are found for the U-N and U-O interaction in the anionic ligand case, with similarly high LBOs for the U-N interaction in the neutral ligand case (0.64) and for the U-N interaction in the positively charged ligand case (0.52).

Table 3. Thermodynamics of U-bis-AO complexes

	UO_2^{2+}		
ΔG (kcal mol^{-1})	bis-AO^{-1}	bis-AO	bis-AO^{+1}
(B) 1 U binding pocket	**-56.124**	**-8.643**	**-5.532**
(D) 2 U binding pocket	**-70.400**	**-21.268**	**-13.860**

Taking into account the mismatch in hardness between the soft, heavy alkali and alkaline earth metal ions and amidoxime as well as their much larger ionic radius relative to uranyl, it was hypothesized that uranyl would be sorbed preferentially to strontium and cesium. The results of the DFT study suggest that metal ion affinity by the bis-amidoxime functionalized polymer indeed trends as $Cs^+ \approx Sr^{2+} << UO_2^{2+}$. The deprotonated form of the bis-amidoxime ligand was the only case where complexation with Sr^{2+} was spontaneous at room temperature. Moreover, owing to low metal-ligand LBO values and NPA values close to +2.0 on the metal center, the metal-ligand interaction was expected to be weak and ionic. To compare, all optimized structures with cesium showed NPA values > 0.99 with very little variation in free energy of complexation upon deprotonation. It was also found that the ligand distorts via rotation around the central C-O-C linkage in order to accommodate the Cs^+ in binding pocket geometry. Since this rotation is sterically hindered in the polymeric material, it was thought that cesium binding would be even less favored. Finally, the calculations confirm amidoxime's remarkable affinity for the uranyl dioxocation. Free energies of complexation were exergonic at every geometric configuration and protonation state tested. More importantly, the Gibbs free energy becomes more favorable by ~8 kcal mol^{-1} upon binding another metal ion. In all cesium and strontium cases, multi-metal binding is disfavored at room temperature as evidenced by increasingly positive free energy values. Indeed, in the computed complexes with uranyl, the ligand is able to orient itself in a way that favors strong binding of two metal ions, behavior not apparent in the optimization of Sr^{2+} and Cs^+ complexes above. Bis-amidoxime's strong propensity for the formation of stabilizing interactions with uranyl as determined via DFT is one of the main reasons behind its empirically realized selectivity over strontium and cesium.

The computational results underscore several key ligand features that are necessary to exploit for sequestrations with tandem goals of elemental selectivity and high uptake. First, the amidoxime moiety possesses a strong affinity for uranyl owing to its unique geometry and mixture of N and O donors. Tailoring the energetics of the ligand to the metal of interest is a powerful method to instill high uptake characteristics.[38] Second, ligand pre-organization plays a significant role in metal selectivity. In this work, the diaryl ether was purposely chosen for its intermediate flexibility—less flexible than amidoxime functionalized aliphatic molecules but more flexible than the

analogous functionalized fluorenes and dibenzofurans reported in the literature to possess high uranium affinity.[48,49] Moreover, the presence of several hydrogen bond acceptors allowed for

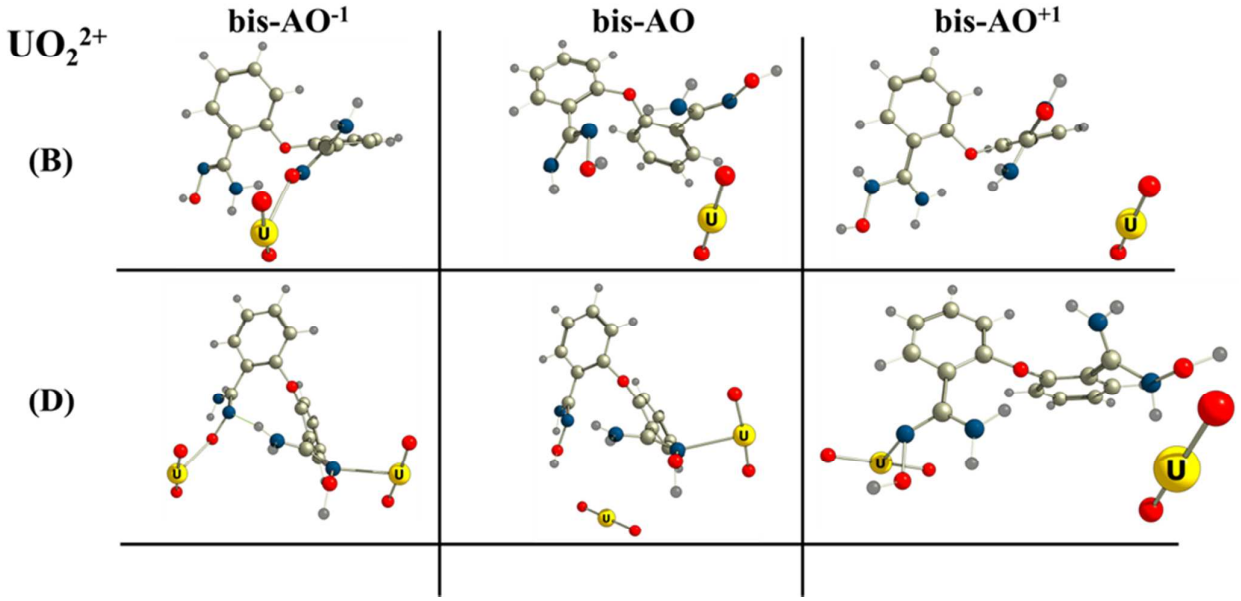

Fig. 3 Geometrically optimized perspective structures of uranium complexes. The gray, dark gray, red, dark blue, and yellow spheres represent C, H, O, N , and U respectively. (B) and (D) series have the same definitions as before, vide ante

the possibility of hydrogen bonding to preserve the orientation of the amidoxime moieties until a suitable metal could be exchanged. Intramolecular hydrogen bonding as a tool to preserve some of the ligand pre-organization without the need for a classic conformationally rigid aromatic backbone allows for stronger binding and correspondingly higher uptake. This characteristic of the ligand is expected to vary with pH, with the extent of intramolecular H-bonding more apparent in acidic solutions. Thus, it is the combined effects of favorable ligand electrostatics and high degree of pre-organization that should allow for selective separations.

Uptake Studies

The *in silico* predictions of the relative stabilities of bis-amidoxime coordination complexes have been tested experimentally via pH-dependent studies of Sr^{2+}, Cs^{+}, and UO_2^{2+} uptake. Depicted in Figure 4, the amidoximated sorbent shows the highest uranium uptake under near-neutral conditions, sorbing upwards of 99% of U from solution in 30 minutes. This is in line with the computation results, which showed uranium uptake is thermodynamically favorable across the pH range probed in the experiments. Strontium uptake is negligible throughout the same pH range and Cs uptake is small (<15%) under acidic conditions and higher (<30%) under basic conditions.

We observe negligible strontium uptake throughout the pH range (Table 4). The low affinity for strontium by the bis-amidoxime ligand is best explained by the positive values obtained for the free energy of complexation as well as small deviations from the NPA on the metal center (indicative of a low degree of ligand to metal charge transfer) as determined via DFT calculations.

Table 4. $^{90}Sr^{2+}$ Uptake

pH	D_W (mL g^{-1})	% Sorbed
2	**20.57**	**2.0**
3	**12.97**	**1.2**
4	**0**	**0**
5	**16.74**	**1.6**
6	**0**	**0**
8	**0**	**0**
9	**0**	**0**
10	**0**	**0**

Cesium uptake is slightly higher at both pH extremes studied, as expected by the similar free energies obtained from computation. Cs^{+} uptake averages 25.6% between pH = 8 and pH = 10 and diminishes to an average of 14% between pH = 2 and pH = 3. Distribution ratios of $3.73 \cdot 10^2$ mL g^{-1} at pH = 8 and $2.26 \cdot 10^2$ mL g^{-1} at pH = 3 represent the highest values within

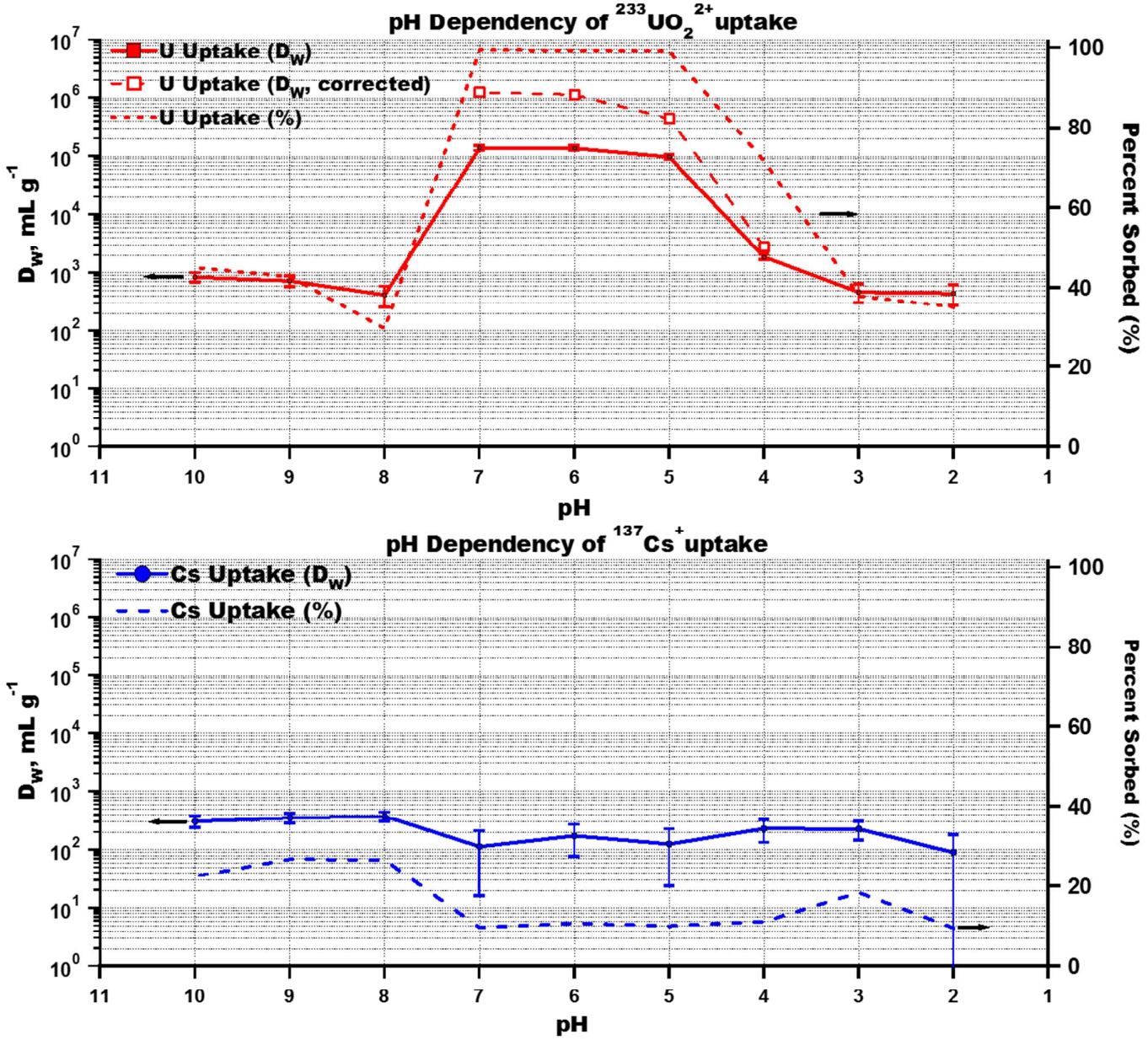

Fig. 4 Acid dependency studies on $^{90}Sr^{2+}$, $^{137}Cs^+$, and $^{233}UO_2^{2+}$ uptake. Experiments conducted at room temperature at a phase ratio of 1 mg sorbent to 1 mL solution with a mixing time of 30 min. Uptake experiments were repeated to determine the error interval. Error bars are depicted for each point as shown.

the high and low pH ranges, respectively. This small amount of cesium that is sorbed by the polymer may be attributed to binding by the methylenebisacrylamide crosslinker used in the preparation of the polymeric material. Several examples of amide-Cs^+ complexes exist in the literature[50–53] and some Cs^+ binding contribution from the C=O of the crosslinker would be expected.

Uranium uptake is moderate to high throughout the pH range studied. Under more basic conditions, we see a leveling off of uranyl uptake with a maximum uptake of 45% (D_W= $\mathbf{8.44 \cdot 10^2}$mL g^{-1} at pH = 10). The drop in uranium uptake under basic conditions could be attributable to buffer effects, since there is an appreciable time dependence in metal uptake (SI Figure S8) and/or to the formation of uranyl hydroxo complexes since the formation of monomeric $UO_2(OH)_2$ and dimeric $(UO_2)_2(OH)_2^{2+}$ species directly

compete with bis-amidoxime complexation at higher pH.[54] Similar behavior is seen under acidic conditions with an average U uptake of 37% between pH = 2 and pH = 3 and a maximum D_W of $\mathbf{4.69 \cdot 10^2}$ mL g^{-1} at pH = 3.

At near neutral pH, the bis-amidoximated material sorbs upwards of 99% of uranium from solution. Calculated distribution ratios are equal to about 10^5 in the pH 5 to 7 range. Correcting for acetate ion complexation by using equation 5, found in the Supporting Information, gives distribution ratios of about 10^6 in that pH range. These results compare very well to amidoxime functionalized porous aromatic framework materials used for uranium from seawater applications. Ma and co-workers[55] calculated a distribution coefficient (functional form equivalent to the distribution ratio discussed herein) of $1.05 \cdot 10^6$ mL g^{-1} for uranium uptake from water at pH = 6 (SI Table S9).

The selectivity of uranium over cesium and strontium stands in direct juxtaposition to certain conventional ion-exchange resins such as Dowex 50-X8 whose affinity for Sr^{2+} over UO_2^{2+} under similar conditions is twice as high.[23] A more direct comparison with other amidoximated polymeric sorbents[55,56] shows that the bis-amidoximated material discussed herein holds a distinct advantage in its selectivity for uranyl over alkali or alkaline earth metals at near neutral conditions. Amidoxime functionalized hydrogel particles developed by Blake and co-workers[56] realize nearly 100% uranium uptake from groundwater solutions spiked with 30 ppb or 1 ppm U in under 5 minutes. However, significant amounts of Na^+ (~100%) and Mg^{2+} (~25%) are also sorbed suggesting poor selectivity of their hydrogel material for uranium in the presence of mono- and divalent cations (SI Table S9).

The bis-amidoxime functionalized polymer also outperforms layered metal sulfide materials both in terms of uptake and selectivity. Using one such material, Sarma *et al.*[14] found distribution coefficients of $5.5 \cdot 10^4$ mL g^{-1} for Cs^+, $3.9 \cdot 10^5$ mL g^{-1} for Sr^{2+}, and $2.7 \cdot 10^4$ mL g^{-1} for UO_2^{2+} from uptake studies conducted in water at pH ~ 7. Distribution ratios obtained using the bis-amidoxime polymer at pH = 6 are $1.8 \cdot 10^1$ mL g^{-1} for Cs^+, 0 mL g^{-1} for Sr^{2+}, and $1.4 \cdot 10^5$ mL g^{-1} for UO_2^{2+} demonstrating this material's high U affinity and selectivity (SI Table S9).

Conclusions

We provide evidence for the selective nature of uranium uptake by bis-amidoxime functionalized polymer materials and compare the computational and experimental results to other state of the art materials.

DFT calculations determined that the bis-amidoxime ligand has poor affinity for both cesium and strontium as evidenced by: (i) Large, positive Gibbs free energies on the order of 3-6 kcal mol^{-1}; (ii) low WBI and LBO ligand-metal bond indices; and (iii) a small deviation from the NPA on each metal center. Uranyl bound ligands, on the other hand, showed favorable binding thermodynamics and significant reductions in the NPA on each metal center. The bis-amidoxime ligand was found to exhibit stabilizing interactions with uranium with little to no affinity for strontium and cesium despite undergoing the same DFT-geometry optimization. Multiple uranium ions can be favorably bound to the bis-amidoxime ligand regardless of the ligand's protonation state. The notion that a singular uranyl binding event enhances bis-amidoxime's affinity for a second uranyl ion[46,47] holds important implications for the design of more effective radionuclide chelators and merits further study.

The amidoximated polymer was found to sorb nearly 100% of ^{233}U from a 0.01 M acetate buffered solution at near neutral pH in 30 minutes.[57] Importantly, ^{90}Sr uptake was insignificant and ^{137}Cs uptake was low under the same conditions corroborating the computational calculations. Moreover, at near neutral pH, the amidoximated polymer is able to decontaminate water to significantly below the 30 ppb U target set by the US Environmental Protection Agency[58] with a starting U concentration of 330 ppb and a final U concentration of 2.6 ppb.

The judicious combination of hydrophilic crosslinker and highly uranophilic ligand as predicted via computational calculations resulted in fast kinetics and uranium selectivity in the <400 ppb regime; both features highly desirable for time-sensitive decontamination applications.

Conflicts of interest

There are no conflicts to declare.

Acknowledgements

This work is supported by the U.S. Department of Energy, Office of Science, Office of Basic Energy Sciences, Division of Chemical Sciences, Biosciences and Geosciences, the Heavy Element Chemistry program, under Contract DE-AC02-06CH11357. We acknowledge Keene Zhang for his helpful notes on Multiwfn and AIMS as well as the University of Chicago Research Computing Center for support of this work. We acknowledge Professor Wenbin Lin at the University of Chicago for preliminary suggestions and support.

Notes and references

The manuscript was written through contributions of all authors. All authors have given approval to the final version of the manuscript.

Acronyms used throughout the manuscript:
ANL = Argonne National Laboratory
Bis-AO = Bis-amidoxime functionalized diaryl ether
CPM = Counts per Minute
DFT = Density Functional Theory
LBO = Laplacian Bond Order
LSC = Liquid Scintillation Counting
MCL =Maximum Contaminant Level
NBO = Natural Bond Orbital
NPA = Natural Population Analysis
Uranyl = UO_2^{2+}
WBI = Wiberg Bond Index

1 C. Kantipuly, S. Katragadda, A. Chow and H. Gesser,

Talanta, 1990, **37**, 491–517.
2 S. Tang, H. Zhang and H. K. Lee, *Anal. Chem.*, 2016, **88**, 228–249.
3 S. Demir, N. K. Brune, J. F. Van Humbeck, J. A. Mason, T. V. Plakhova, S. Wang, G. Tian, S. G. Minasian, T. Tyliszczak, T. Yaita, T. Kobayashi, S. N. Kalmykov, H. Shiwaku, D. K. Shuh and J. R. Long, *ACS Cent. Sci.*, 2016, acscentsci.6b00066.
4 P. Misaelides, D. Fellhauer, X. Gaona, M. Altmaier and H. Geckeis, *J. Radioanal. Nucl. Chem.*, 2017, **311**, 1665–1671.
5 C. Jin, J. Hu, J. Wang, C. Xie, Y. Tong, L. Zhang, J. Zhou, X. Guo and G. Wu, *Adv. Chem. Eng. Sci.*, 2017, **7**, 45–59.
6 J. Xiong, S. Hu, Y. Liu, J. Yu, H. Yu, L. Xie, J. Wen and X. Wang, *ACS Sustain. Chem. Eng.*, 2017, **5**, 1924–1930.
7 J. Kim, C. Tsouris, R. T. Mayes, Y. Oyola, T. Saito, C. J. Janke, S. Dai, E. Schneider and D. Sachde, *Sep. Sci. Technol.*, 2013, **48**, 367–387.
8 F. Endrizzi, C. J. Leggett and L. Rao, *Ind. Eng. Chem. Res.*, 2016, **55**, 4249–4256.
9 M. Piechowicz, C. W. Abney, N. C. Thacker, J. C. Gilhula, Y. Wang, S. S. Veroneau, A. Hu and W. Lin, *ACS Appl. Mater. Interfaces*, 2017, **9**, 27894–27904.
10 M. Carboni, C. W. Abney, S. Liu and W. Lin, *Chem. Sci.*, 2013, **4**, 2396–2402.
11 A. A. Alqadami, M. Naushad, Z. A. Alothman and A. A. Ghfar, *ACS Appl. Mater. Interfaces*, 2017, **9**, 36026–36037.
12 W. Liu, X. Dai, Z. Bai, Y. Wang, Z. Yang, L. Zhang, L. Xu, L. Chen, Y. Li, D. Gui, J. Diwu, J. Wang, R. Zhou, Z. Chai and S. Wang, *Environ. Sci. Technol.*, 2017, **51**, 3911–3921.
13 T. Zheng, Z. Yang, D. Gui, Z. Liu, X. Wang, X. Dai, S. Liu, L. Zhang, Y. Gao, L. Chen, D. Sheng, Y. Wang, J. Diwu, J. Wang, R. Zhou, Z. Chai, T. E. Albrecht-Schmitt and S. Wang, *Nat. Commun.*, 2017, **8**, 15369.
14 D. Sarma, C. D. Malliakas, K. S. Subrahmanyam, S. M. Islam and M. G. Kanatzidis, *Chem. Sci.*, 2016, **7**, 1121–1132.
15 S. Das, Y. Oyola, R. T. Mayes, C. J. Janke, L. J. Kuo, G. Gill, J. R. Wood and S. Dai, *Ind. Eng. Chem. Res.*, 2016, **55**, 4103–4109.
16 M. A. Lashley, N. Mehio, J. W. Nugent, E. Holguin, C.-L. Do-Thanh, V. S. Bryantsev, S. Dai and R. D. Hancock, *Polyhedron*, 2016, **109**, 81–91.
17 R. Chiariza, E. P. Horwitz, S. D. Alexandrators and M. J. Gula, *Sep. Sci. Technol.*, 1997, **32**, 1–35.
18 C. W. Abney, R. T. Mayes, T. Saito and S. Dai, *Chem. Rev.*, 2017, **117**, 13935–14013.
19 T. Hirotsu, S. Katoh, K. Sugasaka, M. Senō and T. Itagaki, *Sep. Sci. Technol.*, 1986, **21**, 1101–1110.
20 H. J. Schenk, L. Astheimer, E. G. G. Witte and K. Schwochau, *Sep. Sci. Technol.*, 1982, **17**, 1293–1308.
21 X. Sun, C. Xu, G. Tian and L. Rao, *Dalt. Trans.*, 2013, **42**, 14621.
22 S. P. Kelley, P. S. Barber, P. H. K. Mullins and R. D. Rogers, *Chem. Commun.*, 2014, **50**, 12504–12507.
23 O. D. Bonner, *J. Phys. Chem.*, 1954, **58**, 318–320.
24 M. J. Frisch, Gaussian 09.
25 C. Lee, W. Yang and R. G. Parr, *Phys. Rev. B*, 1988, **37**, 785–789.
26 A. D. Becke, *J. Chem. Phys.*, 1993, **98**, 5648–5652.
27 A. Boda, S. De, S. M. Ali, S. Tulishetti, S. Khan and J. K. Singh, *J. Mol. Liq.*, 2012, **172**, 110–118.
28 S. M. Ali, *Comput. Theor. Chem.*, 2014, **1034**, 38–52.
29 Y. Yang, M. N. Weaver and K. M. Merz, *J. Phys. Chem. A*, 2009, **113**, 9843–9851.
30 J. L. Sonnenberg, P. J. Hay, R. L. Martin and B. E. Bursten, *Inorg. Chem.*, 2005, **44**, 2255–2262.
31 N. Iché-Tarrat and C. J. Marsden, *J. Phys. Chem. A*, 2008, **112**, 7632–7642.
32 S. Vukovic, L. A. Watson, S. O. Kang, R. Custelcean and B. P. Hay, *Inorg. Chem.*, 2012, **51**, 3855–3859.
33 M. Cossi, N. Rega, G. Scalmani and V. Barone, *J. Comput. Chem.*, 2003, **24**, 669–681.
34 T. Lu and F. Chen, *J. Comput. Chem.*, 2012, **33**, 580–592.
35 V. Vallet, U. Wahlgren and I. Grenthe, *J. Phys. Chem. A*, 2012, **116**, 12373–12380.
36 N. Mehio, B. Williamson, Y. Oyola, R. T. Mayes, C. Janke, S. Brown and S. Dai, *Ind. Eng. Chem. Res.*, 2015, **55**, 4217–4223.
37 N. Mehio, M. a. Lashely, J. W. Nugent, L. Tucker, B. Correia, C.-L. Do-Thanh, S. Dai, R. D. Hancock and V. S. Bryantsev, *J. Phys. Chem. B*, 2015, **119**, 3567–3576.
38 C. W. Abney, S. Liu and W. Lin, *J. Phys. Chem. A*, 2013, **117**, 11558–11565.
39 T. M. Klapötke, T. G. Müller, M. Rusan and J. Stierstorfer, *Zeitschrift für Anorg. und Allg. Chemie*, 2014, **640**, 1347–1354.
40 C.-L. Xiao, Q.-Y. Wu, C.-Z. Wang, Y.-L. Zhao, Z.-F. Chai and W.-Q. Shi, *Inorg. Chem.*, 2014, **53**, 10846–10853.
41 E. Philip Horwitz, R. Chiarizia and M. L. Dietz, *Solvent Extr. Ion Exch.*, 1992, **10**, 313–336.
42 A. Boda, S. M. Ali, M. R. K. Shenoi, H. Rao and S. K. Ghosh, *J. Mol. Model.*, 2011, **17**, 1091–1108.
43 S. Vukovic, L. A. Watson, S. O. Kang, R. Custelcean and B. P. Hay, *Inorg. Chem.*, 2012, **51**, 3855–3859.
44 C. W. Abney, R. T. Mayes, M. Piechowicz, Z. Lin, V. S. Bryantsev, G. M. Veith, S. Dai and W. Lin, *Energy Environ. Sci.*, 2016, **9**, 448–453.
45 J. Kříž, J. Dybal, E. Makrlík, P. Vaňura and B. A. Moyer, *J. Phys. Chem. B*, 2011, **115**, 7578–7587.
46 A. Stemmler, *Angew. Chemie (International ed. English) Commun.*, 1996, **35**, 2841–2843.
47 T. N. Parac-Vogt, A. Pacco, P. Nockemann, Y. F. Yuan, C. Görller-Walrand and K. Binnemans, *Eur. J. Inorg. Chem.*, 2006, 1466–1474.
48 S. Vukovic and B. P. Hay, *Inorg. Chem.*, 2013, **52**, 7805–7810.
49 S. Vukovic, B. P. Hay and V. S. Bryantsev, *Inorg. Chem.*, 2015, **54**, 3995–4001.
50 M. Burgard, M. R. Yaftian, C. Jeunesse, I. Bagatin and D. Matt, *J. Incl. Phenom. Macrocycl. Chem.*, 2000, **38**, 413–421.
51 B. Qin, C. Ren, R. Ye, C. Sun, K. Chiad, X. Chen, Z. Li, F. Xue, H. Su, G. A. Chass and H. Zeng, *J. Am. Chem. Soc.*, 2010, **132**, 9564–9566.
52 Q. He, G. M. Peters, V. M. Lynch and J. L. Sessler, *Angew. Chemie Int. Ed.*, 2017, **56**, 13396–13400.

53 G. Horvat, L. Frkanec, N. Cindro and V. Tomišić, *Phys. Chem. Chem. Phys.*, 2017, **19**, 24316–24329.
54 S. Tsushima and T. Reich, *Chem. Phys. Lett.*, 2001, **347**, 127–132.
55 B. Li, Q. Sun, Y. Zhang, C. W. Abney, B. Aguila, W. Lin and S. Ma, *ACS Appl. Mater. Interfaces*, 2017, **9**, 12511–12517.
56 N. Sahiner, H. Yu, G. Tan, J. He, V. T. John and D. A. Blake, *ACS Appl. Mater. Interfaces*, 2012, **4**, 163–170.
57 O. of W. US Environmental Protection Agency and US Environmental Protection Agency, *Off. Water*, 2001, EPA 816-F-01-003.
58 O. of W. US Environmental Protection Agency, 2001, EPA 816-F-01-003.

TOC Soderholm BisAO Manuscript ID: DT-ART-12-2017-004935

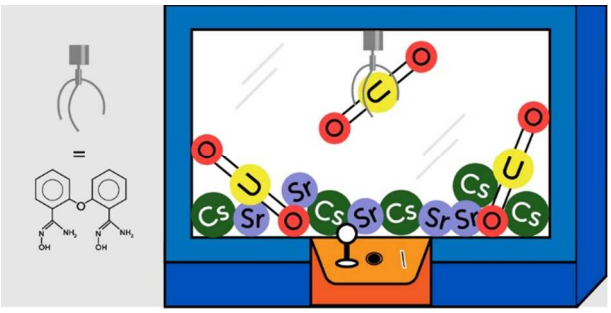

Density functional theory and separations experiments combine to demonstrate the selectivity of bis-amidoxime polymer for uranyl extraction from aqueous solution